Available online at www.sciencedirect.com
ScienceDirect
Trans. Nonferrous Met. Soc. China 31(2021) 371−381
Transactions of Nonferrous Metals Society of China
www.tnmsc.cn

Comprehensive study on quasi-static and dynamic mechanical properties and wear behavior of Mg–B_4C composite compacted at several loading rates through powder metallurgy

K. RAHMANI[1], G. H. MAJZOOBI[1], G. EBRAHIM-ZADEH[2], M. KASHFI[3]

1. Mechanical Engineering Department, Bu-Ali Sina University, Hamedan 65174, Iran;
2. Department of Soil Science, Faculty of Agriculture, Guilan University, Rasht 4199613776, Iran;
3. Mechanical Engineering Department, Ayatollah Boroujerdi University, Boroujerd 6919969737, Iran

Received 3 April 2020; accepted 2 December 2020

Abstract: The present study aims to fabricate and evaluate the mechanical properties and wear behavior of Mg metal matrix composite, reinforced by 0, 1.5, 3, 5 and 10 vol.% B_4C microparticles. Mg−B_4C samples were fabricated at 450 °C and under different loading rates by using split Hopkinson bar (SHB), drop hammer (DH) and Instron (QS) at strain rates of 1600, 800 and 0.008 s^{-1}, respectively. The mechanical properties including microhardness, quasi-static and dynamic compressive strengths and wear behavior of samples were experimentally investigated. The results show that, the hardness of SHB and DH samples is obtained to be 20.2% and 5.7% higher than that of the QS sample, respectively. The wear rate and wear mass loss of Mg–10.0%B_4C samples fabricated by SHB were determined lower than those of the QS sample by nearly 33% and 39%, respectively. The quasi-static compressive strengths of Mg−5.0%B_4C are improved by 39%, 30% and 29% for the SHB, DH and QS samples, respectively, in comparison with the case of pure Mg. Furthermore, it is discovered that the dynamic compressive strength of samples is 51%−110% higher than their quasi-static value with respect to the B_4C content.

Key words: powder compaction; high strain rate; Mg−B_4C composite; hardness; mechanical properties; wear behavior

1 Introduction

Nowadays, the modern world is moving towards a new era in which the application of lightweight materials gets the benefit of high wear resistance. There is a large demand in automobile industries for tribological parts (such as brakes, piston rings and cylinders) and lightweight materials [1,2]. Hence, Mg, as a lightweight structural material, is actively considered for structural applications such as automotive engines, aerospace industry, bicycle frames, computer hardware, biomedical structures, helicopter transmission casings, gearboxes and portable electronic equipment [3,4].

In the past few decades, aluminium alloys have been considered the most promising materials for weight reduction in automobiles [5,6]. More recently, the use of Mg alloys has been increased for weight reduction purposes due to their low density in comparison with aluminium alloys [7]. Mg alloys, however, have shown a relatively low mechanical strength in comparison with the other structural metals, especially at elevated temperatures [8]. Thus, numerous attempts have been performed to improve the mechanical properties of Mg alloys by reinforcing with various micro- and nano-particles such as SiC [9], Al_2O_3 [10] and B_4C [11].

Corresponding author: K. RAHMANI; Tel: +98-912-2820542; E-mail: k.rahmani@basu.ac.ir, rahmanii.kaveh@gmail.com
DOI: 10.1016/S1003-6326(21)65502-4

JIANG et al [11] investigated the fabrication process of Mg−B_4C composite using the powder metallurgy method. They reported an improvement in the hardness and wear resistance of samples reinforced by 10%−20% B_4C. AYDIN et al [12] studied the effect of B_4C and B particle reinforcements on the mechanical properties of Mg−B_4C and Mg−B composites using powder metallurgy. They showed that these reinforcements could improve the mechanical properties of the fabricated composites. Moreover, YAO et al [13] investigated the hardness and wear behavior of Mg−B_4C metal matrix composites, fabricated by metal-assisted pressureless infiltration method. RAHMANI and MAJZOOBI [14] investigated the effect of reinforcement size on the microstructure and relative density of the Mg−B_4C composite.

Powder metallurgy is believed to be the most appropriate, and consequently the most widely used technique for the fabrication of metal matrix composites [15]. This method may be used under quasi-static conditions, which often require hot sintering after or during the fabrication process [16]. However, powder metallurgy can be conducted through the high-velocity compaction (HVC) by using shockwave consolidation. Very few studies have investigated the dynamic compaction and shock consolidation on the fabricated specimens [17].

It is worthwhile noting that the effect of micro size B_4C reinforcement on the mechanical properties at different strain rates has less been studied for Mg metal matrix composites. In the present work, Mg−B_4C samples are fabricated at different loading rates by using split Hopkinson bar (SHB) and drop hammer (DH) considered as the dynamic compaction and Instron (QS) as the quasi-static compaction techniques. This work aims to study the effect of B_4C microparticles content and compaction loading rates on the material hardness, quasi-static and dynamic compressive strengths and wear behavior of Mg−B_4C samples. Figure 1 illustrates the process of sample fabrication and test program in the present work.

2 Experimental

2.1 Materials

Mg powder with purity of 99.5% and the particle size of 100−200 μm was utilized as the composite matrix. B_4C microparticles with the purity of 99% and the average size of 30 μm were considered as the reinforcing phase. Mg−B_4C powder mixtures were then prepared at different volume fractions of B_4C (0, 1.5%, 3%, 5% and 10%). Figure 2 shows the SEM micrographs of surface morphology of Mg and B_4C particles. It can be seen that the particle sizes are sufficient in an acceptable range.

2.2 Specimen fabrication procedure

Composite samples were produced under three different strain rates of 0.008 (QS), 800 (DH) and 1600 s^{-1} (SHB) based on the procedure described in Ref. [18]. The energy for the compactions at the strain rate of 1000 s^{-1} was supplied by 60 kg dropping weight and 3.5 m dropping height. The required energy for compaction process at the strain rate of 1600 s^{-1} was generated by a split Hopkinson bar. The warm compaction process for the powder metallurgy products was carried out in accordance with instructions reported in Refs. [19−21]. The compaction process was conducted at 450 °C which is almost equal to 75% of the melting point of pure Mg, known as its sintering temperature [17]. This temperature was provided by using a 1200 W ceramic heating element. In addition, MoS_2 was utilized as a lubricant to minimize the frictional force between the prepared powder and internal

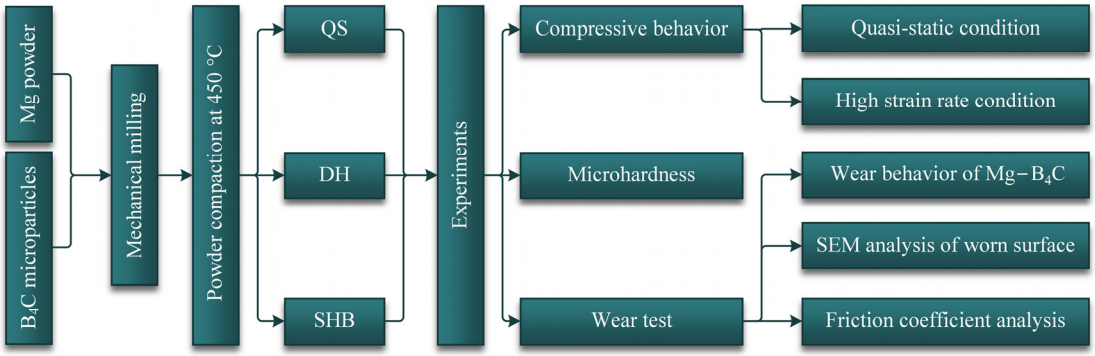

Fig. 1 Process chart of sample fabrication and test program

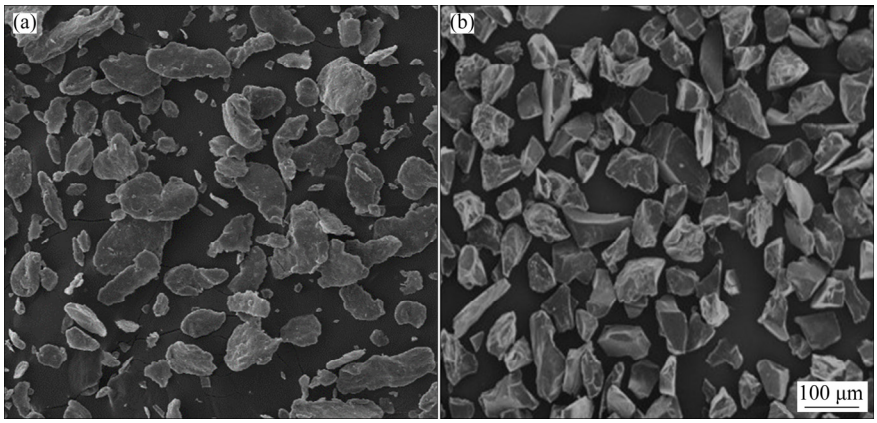

Fig. 2 SEM micrographs of Mg (a) and B_4C (b) particles

surface of compaction die. This lubricant enhances the surface quality of samples and diminishes the roughness of specimen surfaces. After the fabrication process, the cylindrical samples were produced with the length of 10−12 mm (depending on the compaction loading rate) and diameter of 15 mm.

2.3 Experiments

In order to investigate the effects of reinforcement volume fraction on the wear and mechanical properties of Mg−B_4C composites, several experiments were conducted on the produced samples as follows:

(1) SEM test: To investigate the morphology and microstructure of material powders along with the wear mechanism of fabricated samples.

(2) Density of dislocations and grain size characterization: To determine the dislocation density and grain size. The structure of samples was analyzed by an X-ray diffractometer. More details about XRD could be found in Ref. [22].

(3) Microhardness test: To obtain Vicker's hardness of samples according to ASTM-E384 by applying 0.98 N for 15 s [23].

(4) Wear test: Wear test was carried out with a pin-on-disc test device in accordance with ASTM G99−05 under 20 N load for worn distances of 250 and 500 m with the slip velocity of 0.09 m/s [24].

(5) Quasi-static compression test: The conventional compression test was carried out under quasi-static condition by using Instron test machine.

(6) Dynamic compression test: Split Hopkinson pressure bar was employed to obtain the dynamic stress−strain curves of materials at high strain rates [25,26]. Numerous experimental works on the high strain rate response of materials involve the use of the high rate testing apparatus, such as split Hopkinson tension bar [27], split Hopkinson pressure bar [18], and split Hopkinson torsional bar [28].

3 Results and discussion

3.1 Microstructures

SEM micrographs of surface morphology of Mg particles after milling with 5.0 vol.% B_4C particle are depicted in Fig. 3. These images clearly show the uniform distribution of reinforcement particles on the surface of Mg particles after the mechanical milling.

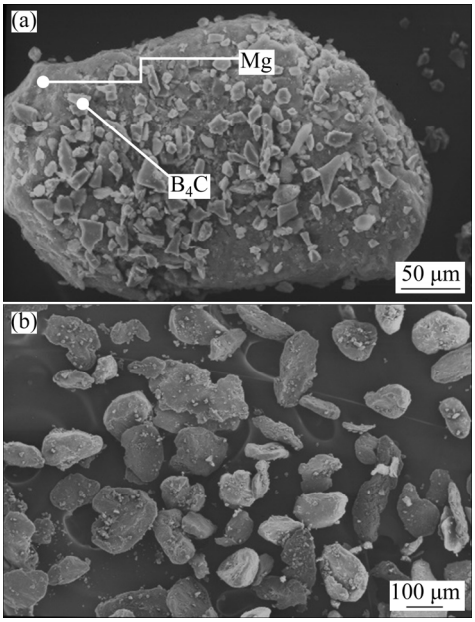

Fig. 3 SEM images of Mg−5.0%B_4C sample after mechanical milling

The SEM micrographs in the backscatter mode and the porosity of composite samples, fabricated by SHB, DH and QS at 450 °C are shown in Fig. 4. As the images clearly demonstrate, by reducing the compaction loading rate, the sample porosity is increased. Figures 4(c_1, c_2) shows the large pores and incomplete compaction in the samples fabricated by QS. The images show that the size of pores and their distances are decreased by changing the manufacturing method from QS to SHB. Furthermore, many pores and grain boundaries disappear in samples compacted by SHB in comparison with QS or DH. Due to the high impact energy, friction effects and adiabatic heating among the powder particles, more powder compaction is achieved for SHB. As it can be seen in Fig. 4, large

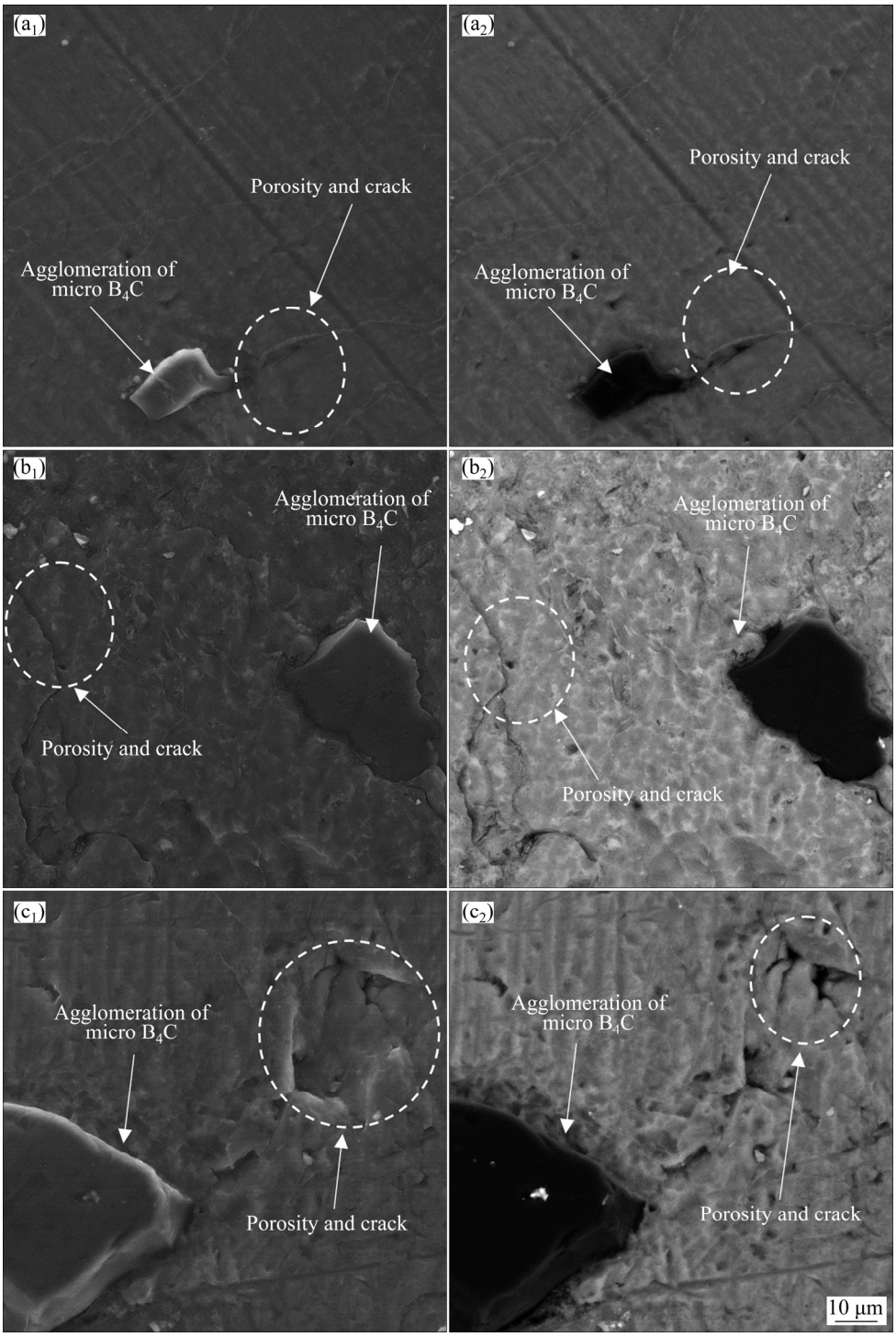

Fig. 4 SEM images (in back scatter mode) of Mg−5.0%B_4C samples fabricated by SHB (a_1, a_2), DH (b_1, b_2) and QS (c_1, c_2)

pores have not vanished in the samples fabricated by QS. Therefore, it is hard to eliminate the relatively large gap among the powder particles (large pores). This implies that the sintering process is not adequately performed [29].

3.2 Density of dislocations and grain size

In order to determine the dislocation density and grain size of the samples, their structure was analyzed by an X-ray diffractometer. Figure 5 shows the XRD patterns of Mg−5.0%B_4C specimen fabricated by performing different compaction methods.

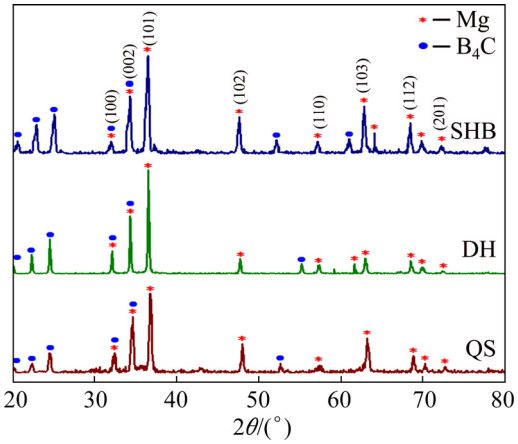

Fig. 5 XRD patterns of Mg−5.0%B_4C samples fabricated by SHB, DH and QS

The dislocation density (δ) is defined as the length of dislocation lines per crystal unit volume which is calculated using Williamson−Smallman relation [30]:

$$\delta=1/D^2 \quad (1)$$

where D is the crystallite size determined by Scherer formula from the full-width at half-maximum (FWHM) and reads [31]

$$D=k\lambda/(\beta\cos\theta) \quad (2)$$

Here, k (=0.9) denotes the shape factor, λ (=1.5418 Å) is the wavelength for Cu K_α radiation, β stands for FWHM and θ is the position of each peak. This procedure is repeated for all peaks and the average grain size is then determined.

The grain size and dislocation densities estimated by XRD are given in Table 1. Once the compaction method is changed from QS to SHB, the Mg crystallite size is reduced from 39 to 19 nm. The decrease of crystallite size is believed to be due to thermomechanical deformation of Mg in the vicinity of B_4C particles during the compaction process. RASHAD et al [32] also attributed the grain size reduction of Mg matrix after the addition of Ti+Al microparticles during the hot extrusion to the recrystallization. The severe changes in crystallite size can also be attributed to the dynamic compaction. The applied impact stress aids dislocations to annihilate and facilitate the material recrystallization [33].

Table 1 Grain size and dislocation density of Mg−5.0%B_4C samples measured by XRD

Sample code	Grain size/nm	δ/m^{-2}
QS	39.7565	6.3267×10^{14}
DH	23.8812	17.5341×10^{14}
SHB	19.0311	27.6101×10^{14}

The dislocation density of samples fabricated by QS is obtained lower than the two others. By adding the reinforcing phase, both Orowan and dislocation density strengthening effects are considerably increased. This increase in the dislocation densities of specimens is believed to be due to some strengthening mechanisms such as Orowan mechanism and thermal mismatch of Mg and B_4C particles. Table 1 shows that an increase of 39% and 29% in the dislocation densities of samples fabricated by DH and SHB is obtained in comparison with QS, respectively.

3.3 Microhardness

The variation in microhardness of samples fabricated by different volume fractions of B_4C microparticles is illustrated in Fig. 6. As it can be seen, the average hardness is enhanced by increasing the volume fraction of B_4C. This increase in hardness is observed to be higher in samples fabricated by using dynamic rather than quasi-static compaction. The results indicate that the addition of microparticles enhances the hardness of Mg−10.0%B_4C samples by 33%, 26% and 19% with SHB, DH and QS, respectively, in comparison with the case of pure Mg.

This improvement in hardness can be elaborated through the following reasons: (1) the hardness of reinforcement particles, (2) the presence of harder B_4C particles as a barrier for local deformation during compaction (hardening effects of B_4C particles), and (3) decrease in grain

size due to the dynamic recrystallization [34]. The latter is speculated as a result of reinforcing phase hardening effect and its intrinsic hardness.

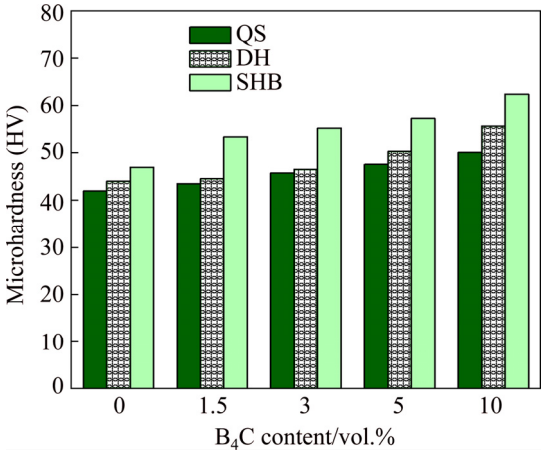

Fig. 6 Variation of microhardness of Mg−B_4C samples compacted by QS, DH and SHB with different volume fractions of B_4C

The yield strength and hardness are related to each other through the well-known Tabor equation (σ_y=H/3). Thus, improvement of hardness can be an indication of material strength enhancement with the increase of reinforcement content [35]. The maximum hardness is obtained in samples fabricated by SHB method as it creates a stronger bonding. During the dynamic compaction, the induced stress wave produces severe local plastic deformations among powder particles. Considering the friction among powder particles, significant thermal energy is generated during the compaction process. As it can be observed in Fig. 6, the compaction method and B_4C volume fraction can affect the microhardness of compacted samples.

3.4 Quasi-static compressive strength

The compressive engineering stress−strain curves of pure Mg and Mg−B_4C samples fabricated by SHB, DH and QS are shown in Fig. 7. The quasi-static compressive engineering stress−strain curves for samples fabricated by SHB are shown in Fig. 7(a). It is shown that the most improvement of quasi-static compressive strength is obtained for Mg−5.0%B_4C. The hardness of B_4C microparticles and a thin layer of Mg oxide (MgO) covering the Mg particles operate as the reinforcement phases and result in a comprehensive strength improvement of the specimen [36]. Furthermore, some of strengthening mechanisms such as Orowan and thermal expansion coefficient mismatch (28.4×10^{-6} K^{-1} for Mg and 5×10^{-6} K^{-1} for B_4C [37,38], lead to the formation of dislocations which can enhance the material strength.

As Fig. 7(b) suggests, the highest compressive strength is observed in the Mg–5.0%B_4C as it is enhanced by about 28% in comparison with the pure Mg. The decrease in quasi-static compressive

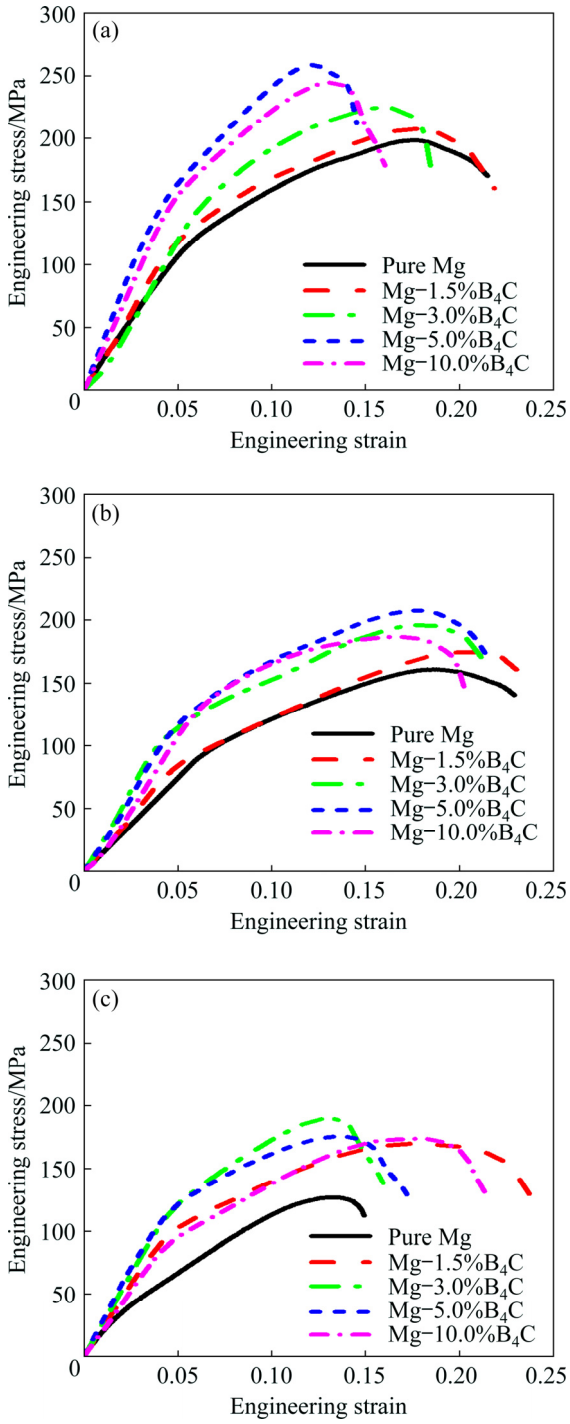

Fig. 7 Quasi-static compressive engineering stress−strain curves of pure Mg and Mg–B_4C samples fabricated by SHB (a), DH (b) and QS (c)

strength for the higher B_4C volume fraction occurs as a result of the formation of more pores and clustering of microparticles. Moreover, increasing the content of hard particles in a ductile matrix reduces the composite pressability. As harder particles distribute in the Mg matrix, they can act as stress concentration locations. By limiting the plastic deformations, microparticles can act as a barrier for improving the strength and formability of composites. The pile-up of particles among Mg particles can be considered as a major factor for the reduction of sample strength.

The quasi-static compressive strength of QS sample is also enhanced with increasing the content of B_4C microparticles (see Fig. 7(c)). This increase (by 49.5%) is only observed up to 3 vol.% B_4C microparticles. This behavior stems from the different distributions of B_4C and various bondings among B_4C microparticles. Inappropriate mechanical behavior of samples fabricated by QS compared with other samples can be due to low sintering level and insufficient bonds between matrix and reinforcement particles, leading to insufficient local heating in QS.

A comparison between the compressive strength of Mg−B_4C samples fabricated by different compaction methods is presented in Fig. 8. It is shown that the strength of samples fabricated by SHB is averagely higher than similar samples fabricated by DH or QS. This behavior is observed because of higher energy transferred to the powder owing to the imposed higher impact velocity. Furthermore, SEM micrograph of compacted specimens by SHB at 450 °C for different contents of B_4C demonstrates that the addition of B_4C particles gives rise to the appearance of porosity in the fabricated samples.

During the dynamic compaction and according to the well-known kinetic energy equation, $E=mv^2/2$, the delivered kinetic energy to the specimen is increased with the impact velocity. The fine particles are pushed into the spaces between the coarse particles, leading to the reduction of the porosity. Additionally, friction and displacement of the powder particles generate localized heat, leading to some plastic deformations. This thermal energy generates a softened or molten layer that in turn enhances the bonding between the particles. This mechanism consequently increases the green density and the compressive strength of the sample [18]. In addition, Fig. 8 demonstrates that the highest strength is observed in Mg−5.0%B_4C, fabricated by SHB. Its strength is about 24% and 47% higher than that of similar samples fabricated by DH and QS, respectively.

3.5 Dynamic compressive strength

The dynamic compressive stress−strain curves of Mg−B_4C composites fabricated by SHB with different volume fractions of B_4C are experimentally evaluated. A bar chart of the dynamic compressive strength of composite samples with different B_4C contents fabricated by different compaction methods is also illustrated in Fig. 9. The highest dynamic compressive strength is obtained for Mg–5.0%B_4C sample fabricated by SHB, which is determined 18.8% higher than the strength of pure Mg.

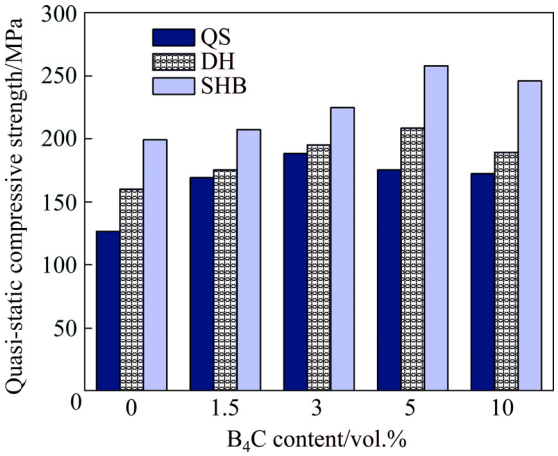

Fig. 8 Comparison of quasi-static compressive strength of Mg−B_4C samples fabricated by SHB, DH and QS with different contents of B_4C

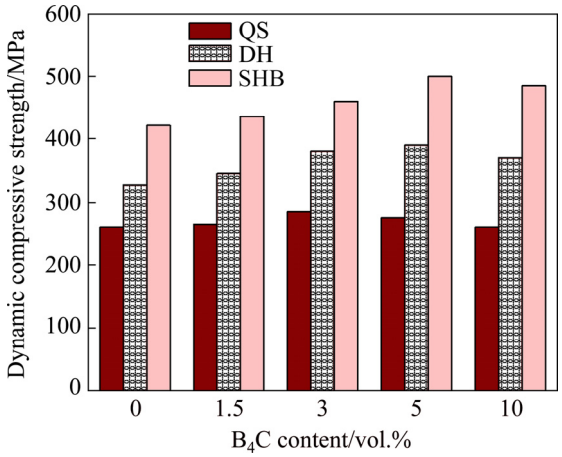

Fig. 9 Comparison of dynamic compressive strength of Mg−B_4C samples fabricated by SHB, DH and QS with different contents of B_4C

By comparing Fig. 8 with Fig. 9, the dynamic compressive strength of Mg–5.0%B_4C samples fabricated by SHB, DH and QS are enhanced by 94%, 88% and 57% in comparison with the quasi-static compressive strength. An improvement in the dynamic and quasi-static compressive strengths is obtained by increasing the B_4C content up to 5 vol.% for the SHB and DH samples. On the other hand, the dynamic and quasi-static compressive strengths of QS samples are enhanced by increasing the B_4C content up to 3 vol.%. It is worth noting that for the higher contents of 5, 5 and 3 vol.% for SHB, DH and QS samples, respectively, no significant improvement is observed.

3.6 Wear resistance

In order to determine the wear resistance of samples fabricated by QS, DH and SHB, required specimens were prepared for conducting pin-on-disk test with the diameter and height of 15 and 12 mm, respectively. During the wear test, different sliding distances play an important role in abrasion of a specimen [39]. Figure 10 shows the mass reduction of SHB, DH and QS samples with the applied force of 20 N. In addition, the mass reduction is increased by amending the distance from 250 to 500 m for all samples while it is reduced by increasing the B_4C content. Although the highest wear rate is observed in QS sample, the least abrasion is obtained for SHB. This implies that the wear mass loss is reduced when the compaction loading rate is increased. Furthermore, by increasing B_4C content from 0 to 10 vol.%, the wear mass loss is reduced by 35.8%, 44.01% and 37.8% for SHB, DH and QS samples, respectively, with the sliding distance of 500 m. The higher wear resistance of SHB sample is associated with the higher hardness and stronger bonds between B_4C and Mg particles, which is facilitated by the load transfer from matrix and reinforcement phases [40].

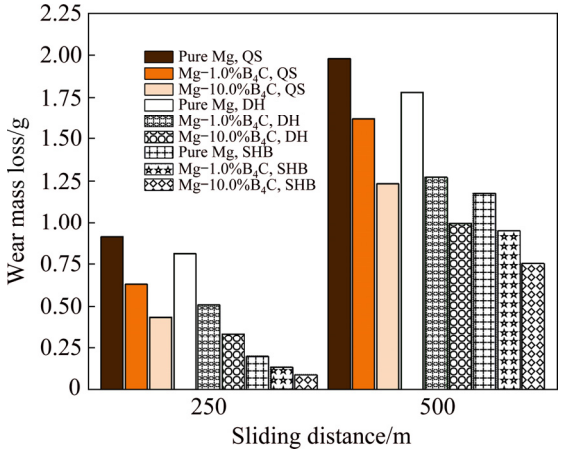

Fig. 10 Variation of wear mass loss of Mg–B_4C samples fabricated by QS, DH and SHB with different sliding distances

The wear rates of SHB, DH and QS samples with 250 and 500 m sliding distances are presented in Fig. 11. It is suggested that, by increasing the B_4C content, the wear rate is clearly reduced. Furthermore, the wear rate is decreased for all samples by increasing the compaction loading rate. For instance, the wear rate reduction of SHB sample without reinforcement particles is around 41% lower than that of the corresponding QS sample.

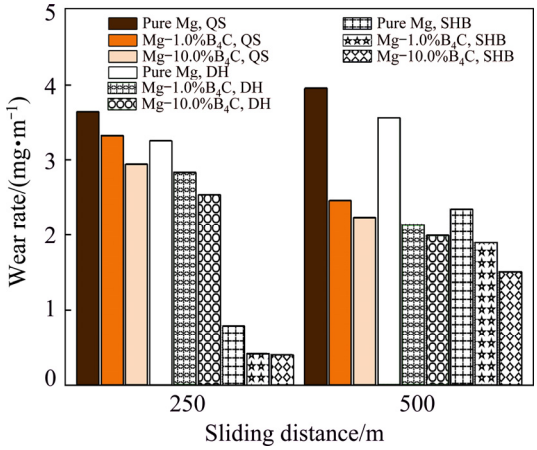

Fig. 11 Variation of wear rate of Mg–B_4C samples fabricated by QS, DH and SHB with different sliding distances

3.6.1 SEM analysis results of worn surface

The surface of specimens is analyzed by SEM images in order to determine their wear behavior. By increasing the compaction loading rate, the width of grooves in the abrasion path is reduced. Moreover, the grooves in the SHB sample are observed to be smaller than those in DH or QS samples.

Figure 12 shows SEM micrographs of wear track of Mg–5.0%B_4C samples fabricated by SHB, DH and QS. Deeper grooves and craters and more delamination on the QS sample surface are observed in comparison with those on DH and SHB samples. Due to the adhesive friction, more material removal from the sample surface occurs, which implies that the abrasion rate is increased. In addition, fewer grooves and craters are seen for the

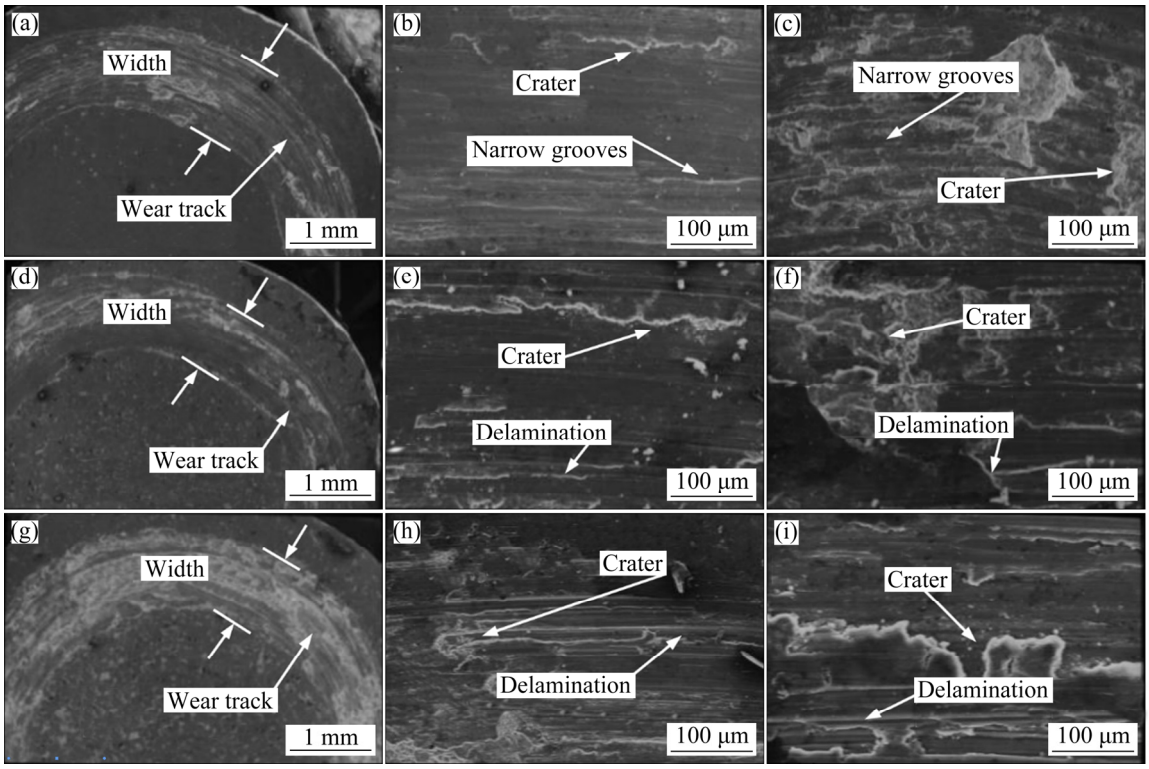

Fig. 12 SEM micrographs of wear track of Mg–5.0%B_4C samples fabricated by SHB (a−c), DH (b−f) and QS (g−i)

Mg–5.0%B_4C sample fabricated by SHB in comparison with those in DH and QS samples.

3.6.2 Friction coefficient

The variation of friction coefficients versus wear distance of Mg–5.0%B_4C samples fabricated by SHB, DH and QS is illustrated in Fig. 13. By increasing the compaction loading rate, the average friction coefficient is reduced from 0.32 to 0.29 for Mg–5.0%B_4C. In general, the reduction of friction coefficient is considered due to the high hardness of reinforcement and the low hardness of interface between pin and sample surface [41]. Tremendous compaction energy in SHB method provides several strong bonds between Mg and B_4C in comparison that in QS and DH. Moreover, the low tendency toward adhesive friction during the sample abrasion leads to low friction coefficient for the SHB sample.

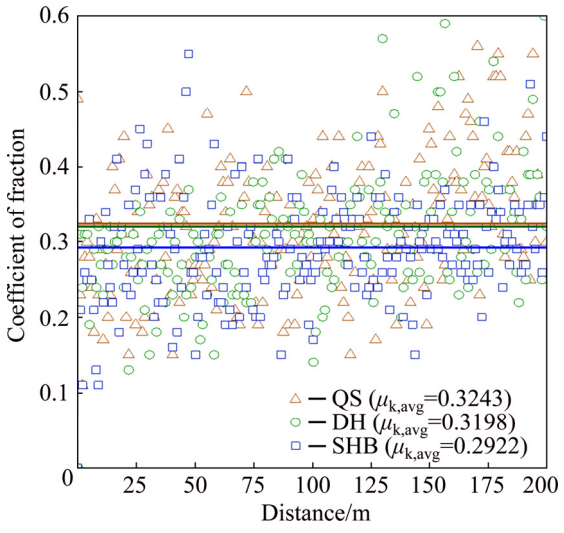

Fig. 13 Variation of friction coefficient versus distance for Mg–5.0%B_4C samples fabricated by SHB, DH and QS

4 Conclusions

(1) The quasi-static compressive strengths are improved for Mg–5.0%B_4C by 39%, 30% and 29% for the QS, DH and SHB samples, respectively, in comparison with the strength for the pure Mg. The highest quasi-static compressive strength is achieved for the SHB sample, which is 47% higher than that of the corresponding QS sample.

(2) The dynamic compressive strengths were enhanced for Mg–5.0%B_4C by 6%, 19% and 18% for the QS, DH and SHB samples, respectively, in comparison with the strength for the pure Mg.

(3) The hardness of Mg–10.0%B_4C samples fabricated by SHB, DH and QS is measured to be

33%, 26% and 19%, respectively, higher than that of the pure Mg. In addition, the wear rate and friction coefficient of Mg–10.0%B_4C sample fabricated by SHB are nearly 33% and 9.5%, respectively, lower than those of QS sample.

References

[1] AATTHISUGAN I, ROSE A R, JEBADURAI D S. Mechanical and wear behaviour of AZ91D magnesium matrix hybrid composite reinforced with boron carbide and graphite [J]. Journal of Magnesium and Alloys, 2017, 5(1): 20−25.

[2] HASHEMI S J, SADOOGHI A, RAHMANI K, DAVARZANI F, AKBARI S. Investigation on the mechanical behavior of fiber−metal laminates based on polyvinyl chloride reinforced by 3D glass fibers [J]. Materials Today Communications, 2020, 25: 101273.

[3] KRISHNAN M N, SURESH S, VETTIVEL S. Characterization, formability, various stresses and failure analysis on workability of sintered Mg−5%B_4C composite under triaxial stress state condition [J]. Journal of Alloys and Compounds, 2018, 747: 324−339.

[4] NAVANEETHA KRISHNAN M, SURESH S, VETTIVEL S. Effects on micro-surface texturing of Mg/B_4C matrix composites under dry sliding wear condition [J]. Transactions of the Indian Institute of Metals, 2020, 73(4): 1−16.

[5] KASHFI M, MAJZOOBI G H, BONORA N, IANNITTI G, RUGGIERO A, KHADEMI E. A new overall nonlinear damage model for fiber metal laminates based on continuum damage mechanics [J]. Engineering Fracture Mechanics, 2019, 206: 21−33.

[6] MAJZOOBI G H, KASHFI M, BONORA N, IANNITTI G, RUGGIERO A, KHADEMI E. A new constitutive bulk material model to predict the uniaxial tensile nonlinear behavior of fiber metal laminates [J]. The Journal of Strain Analysis for Engineering Design, 2017, 53(1): 26−35.

[7] LINDROOS V, TALVITIE M. Recent advances in metal matrix composites [J]. Journal of Materials Processing Technology, 1995, 53(1−2): 273−284.

[8] MORDIKE B, EBERT T. Magnesium: Properties−applications−potential [J]. Materials Science and Engineering A, 2001, 302(1): 37−45.

[9] MAJZOOBI G H, RAHMANI K, KASHFI M. The effect of pre-compaction on properties of Mg/SiC nanocomposites compacted at high strain rates [J]. Journal of Stress Analysis, 2020, 4(2): 19−28.

[10] RAHMANI K, SADOOGHI A, HASHEMI S. The effect of Al_2O_3 content on tribology and corrosion properties of Mg−Al_2O_3 nanocomposites produced by single and double-action press [J]. Materials Chemistry and Physics, 2020, 250: 123058.

[11] JIANG Q, WANG H, MA B X, WANG Y, ZHAO F. Fabrication of B_4C particulate reinforced magnesium matrix composite by powder metallurgy [J]. Journal of Alloys and Compounds, 2005, 386(1−2): 177−181.

[12] AYDIN M, KOÇ R, AKKOYUNLU A. Fabrication and characterisation of Mg−nano B_4C and B composites by powder metallurgy method [J]. Advances in Materials and Processing Technologies, 2015, 1(1−2): 181−191.

[13] YAO Y T, JIANG L, FU G F, CHEN L Q. Wear behavior and mechanism of B_4C reinforced Mg-matrix composites fabricated by metal-assisted pressureless infiltration technique [J]. Transactions of Nonferrous Metals Society of China, 2015, 25(8): 2543−2548.

[14] RAHMANI K, MAJZOOBI G H. The effect of particle size on microstructure, relative density and indentation load of Mg−B_4C composites fabricated at different loading rates [J]. Journal of Composite Materials, 2020, 54(17): 2297−2311.

[15] RAHMANI K, SADOOGHI A, NOKHBEROOSTA M. The effect of the double-action pressure on the physical, mechanical and tribology properties of Mg−WO_3 nanocomposites [J]. Journal of Materials Research and Technology, 2019, 9(1): 1104−1118.

[16] RAHMANI K, MAJZOOBI G H. An investigation on SiC volume fraction and temperature on static and dynamic behavior of Mg−SiC nanocomposite fabricated by powder metallurgy [J]. Modares Mechanical Engineering, 2018, 18(3): 361−368.

[17] FARUQUI A N, MANIKANDAN P, SATO T, MITSUNO Y, HOKAMOTO K. Mechanical milling and synthesis of Mg−SiC composites using underwater shock consolidation [J]. Metals and Materials International, 2012, 18(1): 157−163.

[18] MAJZOOBI G H, RAHMANI K. Mechanical characterization of Mg−B_4C nanocomposite fabricated at different strain rates [J]. International Journal of Minerals, Metallurgy and Materials, 2020, 27(2): 252−263.

[19] SIMCHI A, NOJOOMI A. Warm compaction of metallic powders [M]. Elsevier, 2013.

[20] LEE P, TRUDEL Y, IACOCCA R, GERMAN R, FERGUSON B, EISEN W, MOYER K. Warm compaction [J]. Powder Metal Technologies and Applications, 1998, 7: 376−381.

[21] SAMAL P, NEWKIRK J. Warm compaction and warm die compaction [M]. ASM International, 2015.

[22] RAHMANI K, MAJZOOBI G H, SADOOGHI A, KASHFI M. Mechanical and physical characterization of Mg−TiO_2 and Mg−ZrO_2 nanocomposites produced by hot-pressing [J]. Materials Chemistry and Physics, 2020, 246: 122844.

[23] ASTM E384−00. Test Method for Microindentation Hardness of Materials [S]. ASTM International, 2003.

[24] G99-0.5 Standard test method for wear testing with a pin-on-disk apparatus [S]. ASTM International, 2010.

[25] HAGEMEYER J, REGALBUTO J. Dynamic compaction of metal powders with a high velocity impact device [R]. Fort Worth, Tex: General Dynamics Corp, 1968.

[26] CHEN W W, SONG B. Split hopkinson (Kolsky) bar: Design, testing and applications [M]. Springer Science & Business Media, 2010.

[27] HARDING J, WOOD E, CAMPBELL J. Tensile testing of materials at impact rates of strain [J]. Journal of Mechanical Engineering Science, 1960, 2(2): 88−96.

[28] MAJZOOBI G H, RAHMANI K, LAHMI S. Determination

of length to diameter ratio of the bars in torsional Split Hopkinson bar [J]. Measurement, 2019, 143: 144−154.
[29] KIM J, HA J H, LEE J, SONG I H. Optimization for permeability and electrical resistance of porous alumina-based ceramics [J]. Journal of the Korean Ceramic Society, 2016, 53(5): 548−556.
[30] WILLIAMSON G, SMALLMAN R. III. Dislocation densities in some annealed and cold-worked metals from measurements on the X-ray Debye−Scherrer spectrum [J]. Philosophical Magazine, 1956, 1(1): 34−46.
[31] GORDILLO G, FLOREZ J, HERNANDEZ L. Preparation and characterization of CdTe thin films deposited by CSS [J]. Solar Energy Materials and Solar Cells, 1995, 37(3−4): 273−281.
[32] RASHAD M, PAN F, ASIF M, SHE J, ULLAH A. Improved mechanical proprieties of “magnesium based composites” with titanium–aluminum hybrids [J]. Journal of Magnesium and Alloys, 2015, 3(1): 1−9.
[33] PORTER D A, EASTERLING K E, SHERIF M. Phase transformations in metals and alloys [M]. CRC Press, 2009.
[34] HOKAMOTO K, TANAKA S, FUJITA M, ITOH S, MEYERS M, CHEN H C. High temperature shock consolidation of hard ceramic powders [J]. Physica B: Condensed Matter, 1997, 239(1): 1−5.
[35] YI M J, YIN H Q, WANG J Z, YUAN X J, QU X H. Comparative research on high-velocity compaction and conventional rigid die compaction [J]. Frontiers of Materials Science in China, 2009, 3(4): 447.
[36] ZHANG Z, CHEN D L. Consideration of Orowan strengthening effect in particulate-reinforced metal matrix nanocomposites: A model for predicting their yield strength [J]. Scripta Materialia, 2006, 54(7): 1321−1326.
[37] HASSAN S, GUPTA M. Effect of submicron size Al_2O_3 particulates on microstructural and tensile properties of elemental Mg [J]. Journal of Alloys and Compounds, 2008, 457(1−2): 244−250.
[38] BISWAS S, SUWAS S, SIKAND R, GUPTA A K. Analysis of texture evolution in pure magnesium and the magnesium alloy AM30 during rod and tube extrusion [J]. Materials Science and Engineering A, 2011, 528(10−11): 3722−3729.
[39] LIM C, LEO D, ANG J, GUPTA M. Wear of magnesium composites reinforced with nano-sized alumina particulates [J]. Wear, 2005, 259(1): 620−625.
[40] RAHMANI K, MAJZOOBI G H. The effect of compaction loading rate on hardness and wear resistance of Mg−B_4C nanocomposite [J]. Materials Research Express, 2019, 6(12): 125081.
[41] JAFARI M, ENAYATI M, ABBASI M, KARIMZADEH F. Compressive and wear behaviors of bulk nanostructured Al2024 alloy [J]. Materials & Design, 2010, 31(2): 663−669.

粉末冶金 Mg−B_4C 复合材料的准静态、动态力学性能及磨损行为

K. RAHMANI[1], G. H. MAJZOOBI[1], G. EBRAHIM-ZADEH[2], M. KASHFI[3]

1. Mechanical Engineering Department, Bu-Ali Sina University, Hamedan 65174, Iran;
2. Department of Soil Science, Faculty of Agriculture, Guilan University, Rasht 4199613776, Iran;
3. Mechanical Engineering Department, Ayatollah Boroujerdi University, Boroujerd 6919969737, Iran

摘　要：制备体积分数分别为 0、1.5%、3%、5%和 10% B_4C 颗粒增强 Mg 金属基复合材料，研究其力学性能和磨损行为。在 450℃和不同加载速率下，分别采用分离式霍普金森棒(SHB)、锻锤(DH)和 Instron (QS)制备 Mg−B_4C 样品，其应变速率分别为 1600、800 和 0.008 s^{-1}。研究 Mg−B_4C 复合材料的显微硬度、准静态及动态抗压强度等力学性能和磨损性能。结果显示，SHB 和 DH 样品的硬度分别比 QS 样品高 20.2%和 5.7%。SHB 法制备的 Mg−10.0%B_4C 样品的磨损率和磨损质量损失分别比 QS 样品的低 33%和 39%。与纯 Mg 相比，SHB、DH 和 QS 制备的 Mg−5.0%B_4C 样品的准静态抗压强度分别提高 39%、30%和 29%。此外，含 B_4C 样品的动态抗压强度比准静态抗压强度提高 51%~110%。

关键词：粉末压制；高应变速率；Mg–B_4C 复合材料；硬度；力学性能； 磨损行为

(Edited by Bing YANG)